

# Evidence of gate-tunable topological excitations in two-dimensional electron systems

R. Koushik<sup>1</sup>, Matthias Baenninger<sup>2,\*</sup>, Vijay Narayan<sup>1,2</sup>, Subroto Mukerjee<sup>1</sup>,  
Michael Pepper<sup>2,†</sup>, Ian Farrer<sup>2</sup>, David A. Ritchie<sup>2</sup> and Arindam Ghosh<sup>1</sup>

<sup>1</sup> *Department of Physics, Indian Institute of Science, Bangalore 560 012, India and*

<sup>2</sup> *Cavendish laboratory, University of Cambridge,*

*J. J. Thomson Avenue, Cambridge CB3 0HE, UK*

Abstract

arXiv:1005.1379v1 [cond-mat.mes-hall] 9 May 2010

---

\* Present address: Department of Physics, Stanford University, Palo Alto

† Present address: Department of Electronic and Electrical Engineering, University College London, Torrington Place, London WC1E 7JE

Topological defects are ubiquitous from solid state physics to cosmology, where they drive phase transitions by proliferating as domain walls, monopoles or vortices. As quantum excitations, they often display fractional charge and anyonic statistics [1], making them relevant to topologically protected quantum computation [2], but realizing a controlled physical resource for topological excitations has been difficult. Here we report evidence of topological excitations during the localization transition in strongly interacting two-dimensional electron systems (2DESs) in GaAs/AlGaAs heterostructures. We find the electrical conductivity at low electron densities to follow a Berezinskii-Kosterlitz-Thouless (BKT)-like order-disorder transition implying a gate-tunable proliferation of charged topological defects [3, 4]. At low temperatures, a weakening in the temperature dependence of conductivity was observed, and linked to the zero point fluctuations and delocalization of the defects. Our experiments also cast crucial insight on the nature of the ground state in strongly interacting 2DESs in presence of disorder

At low temperatures ( $T$ ), electrical conductivity  $\sigma$  of a disordered 2DES decreases rapidly when the carrier density  $n_s$  is reduced. The dependence of  $\sigma$  on  $n_s$  often reflects the nature of the ground state which is electrically insulating. A classical percolation transition in inhomogenous 2DESs, for example, would cause  $\sigma$  to vary as  $\sim (n_s - n_0)^{4/3}$  for  $n_s > n_0$ , where  $n_0$  is the carrier density at the percolation threshold [5]. When disorder decreases, transition to the insulating state occurs at much lower  $n_s$ , where the inter-particle Coulomb interaction is strong, and corresponds to a large interaction parameter  $r_s = 1/a_B^* \sqrt{\pi n_s} \gg 1$  ( $a_B^*$  is the effective Bohr radius). The nature of the ground state in an interacting 2DES is far from clear, although possibilities of pinned charge-density waves (CDW), such as a Wigner crystal [6–10], charge stripes [11, 12], or other phases [13], have been suggested frequently. Physics of 2DES in this regime offers exotic possibilities such as metallic ground states, diverging effective mass and  $g$ -factors, and so on [9].

In 2D, a CDW state with long range order does not exist at finite  $T$ . However, states with quasi-long range order can exist, which can then undergo phase transitions into a disordered states through BKT type transitions involving the proliferation of topological defects [3, 4, 14–17]. Such transitions can in principle be effected by varying  $T$  or  $n_s$ , and the correlation length ( $\xi$ ) in the disordered state is a non-analytic function of the distance

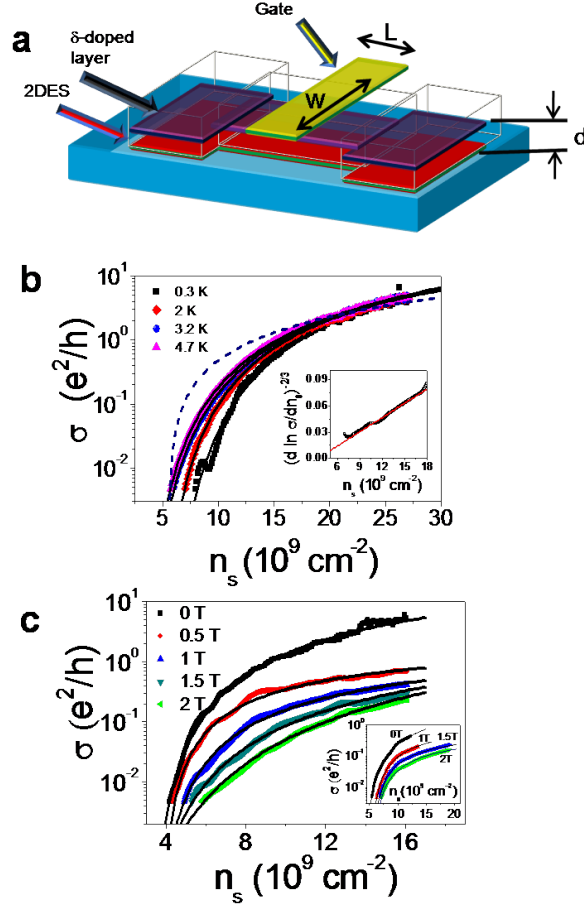
from the phase boundary in density and temperature space:

$$\xi \propto \exp \left[ \frac{A}{(X - X_{KT})^{1/2}} \right] \quad (1)$$

where  $A$  is a constant, and  $X = n_s$  or  $T$ . When  $X > X_{KT}$ , topological defects unbind, resulting in finite conductivity in the otherwise insulating pinned CDW state. The conductivity varies in accordance with the number density  $n_{ex}$  ( $\sim 1/\xi^2$ ) of these defects, although an explicit evidence of this has not been observed until recently [18].

2DESs in modulation-doped GaAs/AlGaAs heterostructures are excellent testing ground for many-body physics, because it allows great control on the level of disorder. Similar to transverse magnetic field ( $H_{\perp}$ ) [8], disorder can also stabilize CDW state, even in the absence of  $H_{\perp}$ , by suppressing the long wavelength fluctuations and arresting the kinetic energy of the electrons [10]. This increases the melting point (*i.e.*  $n_{KT}$  and  $T_{KT}$ ), but excessive disorder may limit the order to very short range, or produce a glassy state, highlighting the need for a subtle balance. We use Si-doped GaAs/AlGaAs heterostructures, where disorder arises from (1) Coulomb potential of ionized Si-atoms, and (2) unintentional background doping. The former component was tuned by using devices from wafers with different setback distances ( $d$ ) between the dopants and the hetero-interface (See Fig. 1a and Methods). It is important to prevent the device from pinching off (*i.e.* turn insulating) at high  $n_s$  which is the case in macroscopic systems with inhomogenous charge distribution [19, 20]. Mesoscopic 2DESs are more suitable since they are relatively insensitive to long range fluctuations in the conduction band [21, 22], and hence form the backbone of our experiments.

The devices were patterned in the form of a microbridge with a crossed metallic surface gate (Fig. 1a) (Ref [22]), limiting the effective area of the device to width of  $\sim 8 \mu\text{m}$  and length  $\sim 0.5 - 4 \mu\text{m}$ . With decreasing  $n_s$  (negative potential on the gate),  $\sigma$  dropped rapidly in all devices, as illustrated in Fig. 1b and c. At low  $T$  ( $\lesssim 0.5$  K), small modulations on overall smooth variation of  $\sigma$  were observed occasionally, which were not reproducible on thermal cycling. Moreover, a percolation transition also failed to describe the  $n_s$ -dependence of  $\sigma$  in our devices (dashed line in Fig. 1b), indicating the influence of inhomogeneity to be small and sporadic. The pinch-off density where  $\sigma \rightarrow 0$ , decreases with increasing  $T$  (shown in Fig. 1b for device C2367), but increases with increasing  $H_{\perp}$  (shown in Fig. 1c for T546 and A2678). The density scale at which pinch-off occurs can be very low,  $n_s \lesssim 2 \times 10^9 \text{ cm}^{-2}$ , corresponding to  $r_s \simeq 13$ , and hence the possibility of a CDW ground state arises naturally.



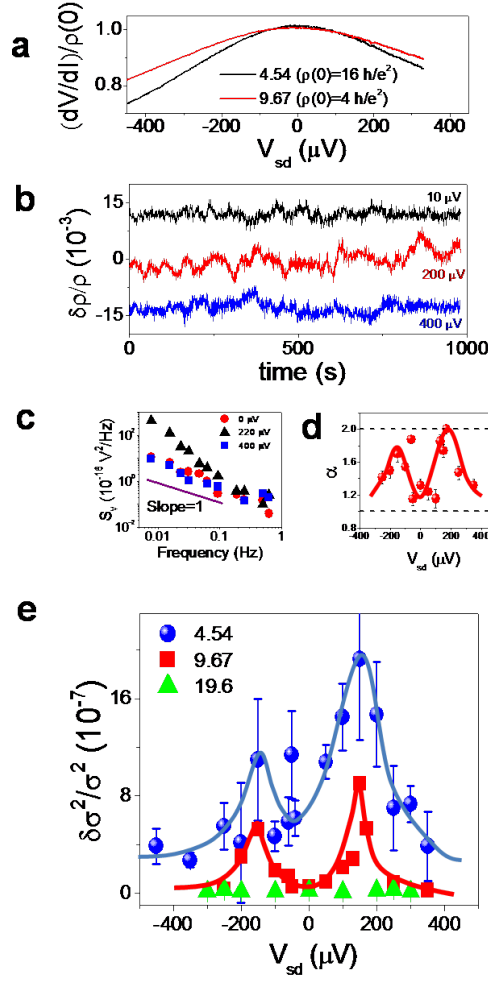
**Figure 1**

FIG. 1: **a)** Schematic of a mesoscopic device geometry showing the 2DEG (red) at the hetero-interface and the dopant layer (light blue). **b)** Conductivity  $\sigma$  (device C2367) as a function of electron density ( $n_s$ ) at different temperatures. The solid black lines are the fits for BKT transition (see Eq. 1 in text). The dashed line represents classical percolation description. The inset shows the linearity of  $(d \ln \sigma / d n_s)^{-2/3}$  in  $n_s$  ( $H_{\perp} = 0 \text{ T}$ ,  $T = 3 \text{ K}$ ) confirming the BKT analysis. The  $x$ -intercept gives the critical density of melting ( $n_{KT}$ ). **c)** Conductivity  $\sigma$  of device T546 vs  $n_s$  at different magnetic fields and  $T = 262 \text{ mK}$ . The fit illustrates the applicability of BKT description (Eq. 1 in text) over several decades in  $\sigma$ . The inset shows similar fits for another device (A2678) with different disorder.

A generic signature of pinned CDW, exploited for 1D Peierls conductors [23], as well as magnetically stabilized 2D electron solids [24], is the broad-band noise (BBN) noise from the electric-field induced thermally activated transitions between the metastable steady states. To explore this possibility, we have measured BBN in our mesoscopic devices in a 4-probe differential (ac + dc) mode, where the differential resistance of the mesoscopic region ( $dV/dI$ ) was measured with a small low-frequency ac modulation (30  $\mu\text{V}$ ) added onto a dc source-drain field ( $V_{sd}$ ). In the insulating regime (resistivity  $\gg h/e^2$ ),  $dV/dI$  decreases, but without any abrupt threshold when  $|V_{sd}|$  increases. This is illustrated for A2678 at  $T = 262$  mK and  $H_{\perp} = 0$  T in Fig. 2a. However, when  $dV/dI$  was recorded as a function of time (over several hours) at fixed  $V_{sd}$ , we observed a random switching noise for  $|V_{sd}| \sim 100 - 200$   $\mu\text{V}$  (see time traces in Fig. 2b). The net variance of noise ( $\delta\sigma^2/\sigma^2$ ) hence shows a peak at a device specific  $V_{sd}$  of  $V_0 \approx 150 - 200$   $\mu\text{V}$ . Away from this regime, the noise is largely featureless with a power spectral density  $\propto 1/f^{\alpha}$  (Fig. 2c), with the spectral exponent  $\alpha \approx 1$  (Fig. 2d), arising from random potential fluctuations at the nearby acceptor sites. As shown in Fig. 2e, the peak in BBN decreases rapidly with increasing  $n_s$ , and in the metallic regime, ( $\sigma \gg e^2/h$ ), it decreases below the measurement background ( $\delta\sigma^2/\sigma^2 \ll 10^{-10}$ ). The nonmonotonicity in noise is unlikely to arise from hopping, or electron glass behavior [25], but can be taken as evidence of electrically driven depinning transition in a pinned CDW [15, 24]. The bias  $V_0$  at the noise maximum represents the depinning threshold which depends on the quenched disorder, and hence only weakly dependent of  $n_s$ . The intermittent plastic flow of the CDW provides the switching noise for which  $\alpha$  is expected to  $\approx 2$  as indeed observed (Fig. 2d).

Evidence of topological defects was subsequently obtained by focusing on  $\sigma$  and scrutinizing its dependence on  $n_s$ . In accordance with Eq. 1, we find  $\sigma = \sigma_0 \exp(-A/\sqrt{n_s - n_{KT}})$  describes the variation of  $\sigma$  over several decades in all devices over a wide range of  $T$  (base to 4.5 K) and  $H_{\perp}$  (see the fits in solid line in Fig. 1b and c where  $\sigma_0$  and  $A$  are constants). This can be readily associated with the proliferation of unbound charged topological defects which dominates electrical conduction in the disordered state ( $n_s > n_{KT}$ ). The self-consistency of the fits was also confirmed by the linearity of  $(d \ln \sigma / dn_s)^{-2/3}$  in  $n_s$  (inset of Fig. 1b), where the  $x$ -axis intercept gives the magnitude of  $n_{KT}$  (within 10% of that obtained from nonlinear fit).

To check if the analysis is physically meaningful, we constructed a melting phase dia-



**Figure 2**

FIG. 2: **a)** Differential resistivity measurements (A2678) as a function of dc source-drain bias ( $V_{sd}$ ) at 0.3 K and two carrier densities ( $10^9 \text{ cm}^{-2}$ ) corresponding to zero-bias resistivities of  $4 h/e^2$  and  $16 h/e^2$ . **b)** Time traces of normalized conductivity fluctuations at three different source-drain bias at  $n_s = 4.54 \times 10^9 \text{ cm}^{-2}$ . Data shows significant broad band noise at bias of  $V_0 \approx 200 \mu\text{V}$ . **c)** The power spectral density (PSD) of conductivity noise at the three bias showing a typical  $1/f^\alpha$  behaviour, where  $\alpha$  is the spectral exponent. **d)** The plot of  $\alpha$  as a function of dc bias which shows a peak magnitude of  $\approx 2$  around  $V_0$ . The solid line is a guide to the eye. **e)** Normalized variance  $\delta\sigma^2/\sigma^2$  as a function of dc bias across the sample at different carrier densities (in units of  $10^9 \text{ cm}^{-2}$ ). The solid lines are guide to eye. The data shows a peak at around  $V_0$  signifying the depinning transition of the pinned electron solid. The peak value decreases at higher densities.

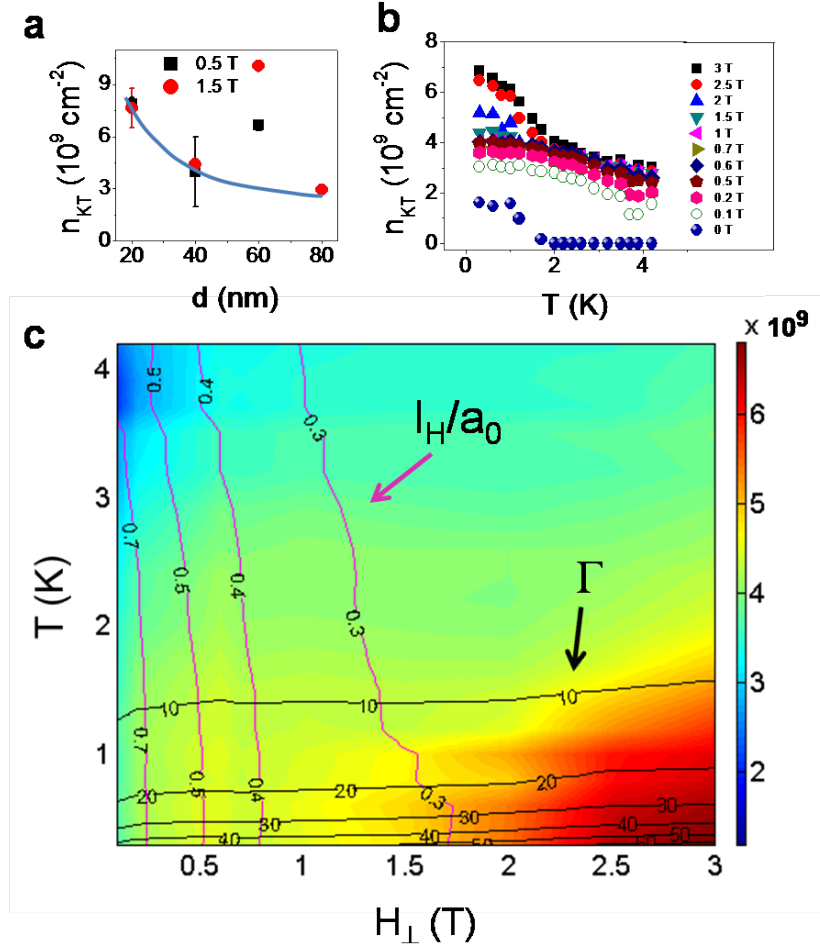


**Figure 3**

FIG. 3: **a)** Critical melting density  $n_{KT}$  (at two magnetic fields) for four samples with different setback distance  $d$  obtained from fitting the BKT (equation 1 text) to conductivity.  $n_{KT}$  decreases with increasing  $d$ , except in C2367 ( $d = 60$  nm) which has a strong background disorder (Methods). **b)** Evolution of  $n_{KT}$  as a function of temperature at different magnetic fields ( $H_{\perp}$ ). **c)** Phase diagram of  $n_{KT}$  in the  $T$ - $H_{\perp}$  space. The magnitude of  $n_{KT}$  is indicated by the scale bar on the right. The quantum fluctuations, characterized by the parameter  $l_H/a_0$  which is the ratio of magnetic length to the inter-site distance, and the classical melting parameter  $\Gamma$  (see text) are evaluated at  $n_{KT}$  and some of the traces are shown. A crossover from quantum to classical melting occurs at higher magnetic fields (bottom right) where  $\Gamma$  approaches  $\approx 80$ .

gram with  $n_{KT}$  extracted from the fits. Disorder quenches the kinetic energy of interacting electrons, and stabilizes the ordered state. Hence, decreasing the spacer thickness  $d$  generally resulted in increasing  $n_{KT}$ , unless the background doping dominates the disorder level. As shown in Fig. 3a,  $n_{KT}$  decreases from A2407 ( $d = 20$  nm) to T546 ( $d = 80$  nm), but abruptly large for C2367 ( $d = 60$  nm) most likely due to strong background doping (see Methods). In a given device though, disorder is fixed and  $n_{KT}$  depends strongly on  $T$  and  $H_{\perp}$ , as illustrated for A2678 in Fig. 3b. Note that at  $H_{\perp} = 0$  T,  $n_{KT}$  is nearly  $1 \times 10^9$  cm $^{-2}$  at low  $T$ , and corresponds to  $r_s \approx 18$  that is much smaller than the expected  $r_s$  for Wigner crystallization in 2DESs without disorder [6].

Fig. 3b illustrates that even a small  $H_{\perp}$  can increase the melting point dramatically by quenching of quantum fluctuations of the constituent “atomic sites”. It agrees with the recent suggestion that melting of a quantum electron solid needs to be addressed in terms of  $l_H/a_0$  rather than  $n_s$  alone [7]. (Here  $l_H = \sqrt{h/eH_{\perp}}$  and  $a_0 = 1/\sqrt{n_s}$  are the magnetic length and mean electron distance, respectively). At higher  $H_{\perp}$  ( $\gtrsim 1.5$  T), a further enhancement in  $n_{KT}$  appears at low  $T$ , pointing towards a different mechanism governing the stability of the CDW. To understand this, we form a surface plot of  $n_{KT}$  in  $T - H_{\perp}$  space, where the traces of constant classical ( $\Gamma = e^2\sqrt{n_s}/4\pi\epsilon_0\epsilon_r k_B T$ ) and quantum ( $l_H/a_0$ ) melting parameters at  $n_s = n_{KT}$  are shown (Fig. 3c). The top-left corner, where both thermal and quantum fluctuations are strongest, the melting occurs at small  $n_{KT}$ , while the bottom-right of the plot represents maximal stability. The abrupt increase in  $n_{KT}$  for  $H_{\perp} \gtrsim 1.5$  T occurs when  $l_H/a_0 \lesssim 0.3$ , signifying very little overlap of neighboring wavefunctions and a crossover from quantum to classical electron solid. Melting in this regime is described by  $\Gamma$ , which approaches  $\sim 80$  in the extreme classical limit ( $H_{\perp} > 2.5$  T), agreeing closely with the estimation of  $\Gamma$  by Thouless for a Wigner crystal [14].

The  $T$ -dependence of  $\sigma$  displays a peculiar weakening below a characteristic temperature scale  $\Theta \sim 1$  K (Fig. 4a-c) which needs further inspection. This behavior is common to all devices, and the magnitude of  $\Theta$  was found to be insensitive to changing device length (over a factor of  $\sim 8$ ), eliminating finite size effect as the cause. The dependence of  $\sigma$  on  $n_s$  also indicates  $n_s$  to be well-defined, and an explanation based on inhomogeneity-related models does not seem to apply here [19, 20]. To understand this quantitatively, we write  $\sigma(T) \propto \exp(-B/\sqrt{T - T_{KT}})f(T)$ . In a “Drude-like” scenario, for instance,  $\sigma(T) \propto n_{ex}(T)\tau(T)$ , where  $n_{ex}(T) \sim \exp(-B/\sqrt{T - T_{KT}})$  and  $f(T)$  would represent the



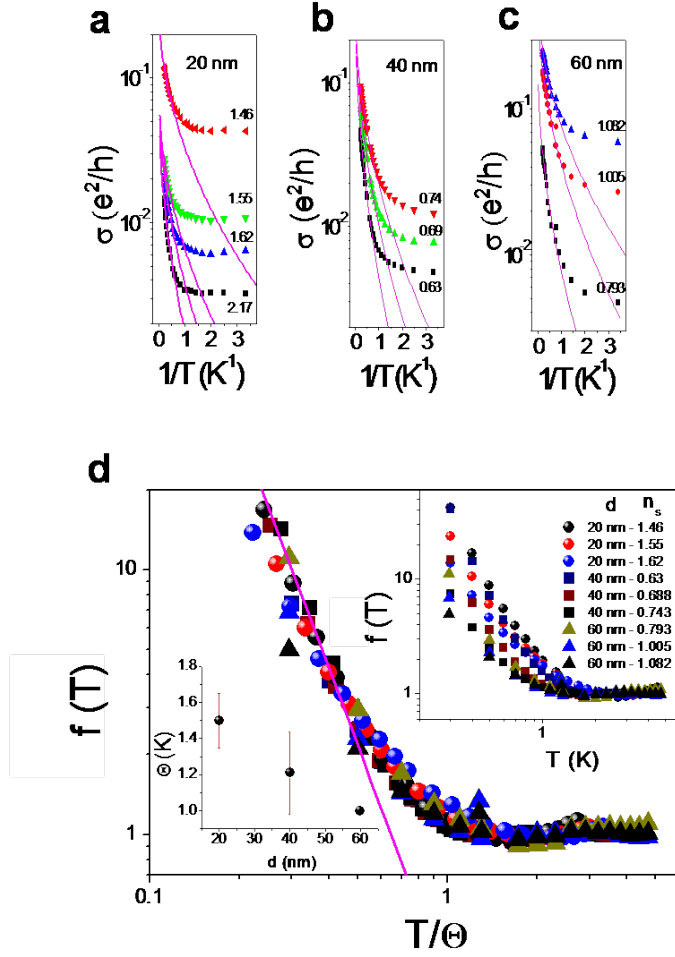


**Figure 4**

FIG. 4: **a)** Temperature dependence of conductivity  $\sigma$  in three devices of different setback distances at various densities (in units of  $10^{10} \text{ cm}^{-2}$ ). The solid lines are fits at the higher temperature range ( $T > 1.5 \text{ K}$ ) for temperature induced BKT transition (Eq. 1). **d)** Scaling of scattering function  $f(T)$  obtained by dividing  $\sigma$  by the BKT fit (see text) for different devices and densities. A single parameter scaling can be observed (holding the parameter  $\Theta$  for A2678 at  $6.3 \times 10^9 \text{ cm}^{-2}$  as reference). The line indicates an asymptotic behaviour of  $f(T) \approx 1/T^3$  for  $T \ll \Theta$ . The top right inset shows experimental  $f(T)$  in various devices at different  $n_s$  ( $10^{10} \text{ cm}^{-2}$ ). The bottom left inset shows the scaling parameter  $\Theta$  to increase with increasing disorder.

temperature dependence of mean scattering time  $\tau(T)$ . The behavior of  $f(T)$  changes at  $T \sim \Theta$ , which was found to be close to the phonon gap of the electron solid through the following analysis: We obtain the domain size  $L_0$  ( $\approx 430$  nm) from the depinning threshold  $V_0$  ( $\sim 200$   $\mu\text{V}$  in BBN measurements for A2678 in Fig. 2) [24], from which the phonon gap could be calculated as  $\sim \hbar c_t/k_B L_0 \approx 1.0$  K (the sound velocity  $c_t \sim 4.7 \times 10^4$   $\text{ms}^{-1}$  is taken to be that of a clean Wigner crystal) [26].

The behavior of  $\sigma(T)$  can be explained if  $\tau(T)$  ( $\sim f(T)$ ) is determined by an Andreev-Lifshitz (AL)-like mechanism of defect-mediated conduction in a quantum solid [27]. For  $T \gg \Theta$ ,  $\tau \rightarrow$  constant, independent of  $T$  due to extensive phonon scattering, and the  $T$ -dependence of  $\sigma$  is determined by that of  $n_{ex}(T)$  only. Hence to extract  $f(T)$ , we fitted  $\sigma(T)$  by  $\exp(-B/\sqrt{T - T_{KT}})$  in the range  $T \gtrsim 1.5$  K (lines in Fig. 4a-c) and subsequently divided it by the fitted trace. The increase in  $f(T)$  for  $T \ll \Theta$  can be readily understood as freeze out of phonons and delocalization of defects as quantum objects with  $\tau \sim 1/T^p$ . A single parameter scaling of the  $T$ -axis collapses  $f(T)$  in all devices onto a universal curve, indicating  $\Theta$  to be the only relevant energy scale (Fig. 4d). We find  $f(T) \sim \tau \sim 1/T^3$  at  $T \ll \Theta$  (line) with  $\Theta$  increasing with increasing disorder (i.e. decreasing  $d$ ) (Fig. 4d(inset)).

Summarizing, there are four key results of this paper: First, both noise measurements and scaling of  $\sigma(n_s)$  indicate a quasi ordered ground state in dilute 2DESs at low  $T$ . The precise nature of ordering is not known, Wigner crystallization being a strong possibility, although it is clear that disorder plays a crucial role in stabilizing such a phase. Second, the BKT scaling provides a new framework within which the transition from strong localization to metallic conduction can be viewed as an order-disorder melting transition. This is in contrast to percolation [5], hopping [28] or Coulomb blockade [29] observed in many experiments over the years (mostly in larger or more disordered 2DESs). Third, the BKT transition also implies existence and proliferation of topological defects in 2DES in semiconductors for the first time with tunable number density. Finally, the scaling of the data described in Fig. 4d suggests that a mechanism like AL may apply here and that the topological defects behave as quantum mechanical entities capable of zero point motion and tunneling.

#### METHODS:

##### **Wafer and device characteristics:**

The devices were fabricated from MBE (molecular beam epitaxy) grown GaAs/ $\text{Al}_{0.33}\text{Ga}_{0.66}\text{As}$  heterostructures, where the two-dimensional electron gas was formed

300 nm below the surface. In all devices, delta (monolayer)-doping of Si ( $\sim 2.5 \times 10^{12} \text{ cm}^{-2}$ ) was implemented. The strength of the disorder is partially determined by the thickness of the spacer layer (undoped  $\text{Al}_{0.33}\text{Ga}_{0.66}\text{As}$ ) situated between the heterostructure interface and dopant layer. The typical as-grown electron mobility was found between  $0.9 - 3 \times 10^6 \text{ cm}^2/\text{V.s}$  at  $n_s \approx 10^{11} \text{ cm}^{-2}$ . The wafers T546 ( $d = 80 \text{ nm}$ ) and C2367 ( $d = 60 \text{ nm}$ ) were grown in different chambers to observe the influence of background doping. The details of various devices used in our experiment are shown in Table 1:

Wafer	$n_D$	$d$	$\mu$	$n_{BG}$
A2407	2.5	20	1.217	0.5
A2678	2.5	40	1.8	0.5
C2367	0.7	60	1.2	1.0
T546	1.9	80	0.9	0.3

**Table 1.** Details of devices used in our measurements showing the doping concentration  $n_D$  ( $10^{12} \text{ cm}^{-2}$ ), spacer thickness  $d$  (nm), as-grown mobility  $\mu$  ( $10^6 \text{ cm}^2/\text{V.s}$ ) and background doping estimate  $n_{BG}$  ( $10^{14} \text{ cm}^{-3}$ ).

### Measurements:

The noise measurements were carried out inside a He-3 cryostat (base electron temperature  $\approx 270 \text{ mK}$ ), using a four-probe ac+dc technique with the ac bias fixed at  $\approx 30 \mu\text{V}$  at an excitation frequency of 128 Hz, and dc bias varied over  $\pm 400 \mu\text{V}$ . The voltage fluctuations across the sample were measured using a lock-in amplifier whose output was subsequently digitized using a 16-bit digitizer, followed by decimation and power spectral density (PSD) calculations using Welch's method of averaged periodogram.

- 
- [1] Laughlin, R.B. Anomalous Quantum Hall Effect: An incompressible quantum fluid with fractionally charged excitations. *Phys. Rev. Lett.* **50**, 1395-1398 (1983).
  - [2] Nayak, C. *et al.* Non-Abelian anyons and topological quantum computation. *Rev. Mod. Phys.* **80**, 1083-1159 (2008).
  - [3] Berezinskii, V.L. Destruction of long-range order in one-dimensional and two-dimensional systems possessing a continuous symmetry group. II. Quantum systems. *Sov. Phys. JETP* **34**, 610-616 (1972).

- [4] Kosterlitz, J.M. & Thouless, D.J. Ordering, metastability and phase-transitions in 2 dimensional systems. *J. Phys. C* **6**, 1181-1203 (1973).
- [5] Das Sarma, S. *et al.* Two-Dimensional Metal-Insulator Transition as a Percolation Transition in a High-Mobility Electron System. *Phys. Rev. Lett.* **94**, 136401 (2005).
- [6] Tanatar, B. & Ceperley, D.M. Ground state of the two-dimensional electron gas. *Phys. Rev. B* **39**, 5005-5016 (1989).
- [7] Chen, Y.P. *et al.* Melting of a 2D quantum electron solid in high magnetic field. *Nat. Phys.* **2**, 452-455 (2006).
- [8] Ye, P.D. *et al.* Correlation lengths of the wigner-crystal order in a two-dimensional electron system at high magnetic fields. *Phys. Rev. Lett.* **89**, 176802 (2002).
- [9] Camjayi, A., Haule, K., Dobrosavljevic, V. & Kotliar, G. Coulomb correlations and the Wigner-Mott transition. *Nat. Phys.* **4**, 932-935 (2008).
- [10] Eguiluz, A.G. & Maradudin, A.A. Two-dimensional Wigner lattice in a magnetic field and in the presence of a random array of pinning centers. *Phys. Rev. B* **27**, 4933-4945 (1983).
- [11] Sambandamurthy, G. *et al.* Observation of pinning mode of stripe phases of 2D systems in high Landau levels. *Phys. Rev. Lett.* **100**, 256801 (2008).
- [12] Koulakov, A.A., Fogler, M.M. & Shklovskii, B.I. Charge density wave in two-dimensional electron liquid in weak magnetic field. *Phys. Rev. Lett.* **76**, 499-502 (1996).
- [13] Spivak, B. & Kivelson, S.A. Phases intermediate between a two-dimensional electron liquid and Wigner crystal. *Phys. Rev. B* **70**, 155114 (2004).
- [14] Thouless, D.J. Melting of the two-dimensional Wigner lattice. *J. Phys. C* **11**, L189-L190 (1978).
- [15] Min-Chul Cha & Fertig, H.A. Topological defects, orientational order, and depinning of the electron solid in a random potential. *Phys. Rev. B* **50**, 14368-14380 (1994).
- [16] Halperin, B. I. & Nelson, D. R., Theory of two dimensional melting. *Phys. Rev. Lett.* **41**, 121 (1978); **E41**, 519 (1978).
- [17] Young, A. P. Melting and the vector Coulomb gas in two dimensions. *Phys. Rev. B* **19**, 1855 (1979).
- [18] Checkelsky, J.G., Lu Li & Ong, N.P. Zero-energy state in graphene in a high magnetic field. *Phys. Rev. Lett.* **100**, 206801 (2008).
- [19] Tripathi, V. & Kennett, M.P. Magnetotransport in disordered delta-doped heterostructures.

- Phys. Rev. B* **74**, 195334 (2006).
- [20] Neilson, D. & Hamilton, A. Tunneling and hopping between domains in the metal-insulator transition in two-dimensions. *Int. Jour. Mod. Phys. B* **22**, 4565-4571 (2008).
- [21] Baenninger, M. *et al.* Local transport in a disordered-stabilized correlated insulating phase. *Phys. Rev. B* **72**, 241311 R (2005).
- [22] Baenninger, M. *et al.* Low-temperature collapse of electron localization in two dimensions. *Phys. Rev. Lett.* **100**, 016805 (2008).
- [23] Bhattacharya, S. *et al.* Origin of broadband noise in charge-density-wave conductors. *Phys. Rev. Lett.* **54**, 2453-2456 (1985).
- [24] Yuan, P. Li. *et al.* Low-frequency noise in the reentrant insulating phase around the 1/5 fractional quantum hall liquid. *Phys. Rev. Lett.* **67**, 1630-1633 (1991).
- [25] Kar, S. *et al.* Observation of non-gaussian conductance fluctuations at low temperatures in Si:P(B) at the metal-insulator transition. *Phys. Rev. Lett.* **91**, 216603 (2003).
- [26] Ferconi, M. & Vignale, G. Theory of the pinning gap in the phonon spectrum of a disordered Wigner crystal. *Phys. Rev. B* **48**, 2831-2834 (1993).
- [27] Andreev, A.F. & Lifshitz, I.M. Quantum theory of defects in crystals. *Sov. Phys. JETP.* **29**, 1107-1113 (1969).
- [28] Van Keuls, F.W. *et al.* Localization scaling relation in two dimensions: Comparison with experiment. *Phys. Rev. B* **56**, 13263-13267 (1997).
- [29] Ghosh, A. *et al.* Density-dependent instabilities in correlated two dimensional electron systems. *J. Phys. Condens. Matter* **16**, 3623-3631 (2004).